UCLA
UCLA Previously Published Works

Title

Enzymatic control of dioxygen binding and functionalization of the flavin cofactor

Permalink

https://escholarship.org/uc/item/3r97v2jn

Journal

Proceedings of the National Academy of Sciences of the United States of America, 115(19)

ISSN

0027-8424

Authors

Saleem-Batcha, Raspudin
Stull, Frederick
Sanders, Jacob N
et al.

Publication Date

2018-05-08

DOI

10.1073/pnas.1801189115

Peer reviewed

Enzymatic control of dioxygen binding and functionalization of the flavin cofactor

Raspudin Saleem-Batcha[a,b], Frederick Stull[c], Jacob N. Sanders[d], Bradley S. Moore[e], Bruce A. Palfey[c,f], K. N. Houk[d,1], and Robin Teufel[a,b,1]

[a]Center for Biological Systems Analysis (ZBSA), University of Freiburg, 79104 Freiburg, Germany; [b]Faculty of Biology, University of Freiburg, 79104 Freiburg, Germany; [c]Program in Chemical Biology, University of Michigan, Ann Arbor, MI 48109; [d]Department of Chemistry and Biochemistry, University of California, Los Angeles, CA 90095; [e]Scripps Institution of Oceanography and Skaggs School of Pharmacy and Pharmaceutical Sciences, University of California, San Diego, La Jolla, CA 92093; and [f]Department of Biological Chemistry, University of Michigan, Ann Arbor, MI 48109

The reactions of enzymes and cofactors with gaseous molecules such as dioxygen (O_2) are challenging to study and remain among the most contentious subjects in biochemistry. To date, it is largely enigmatic how enzymes control and fine-tune their reactions with O_2, as exemplified by the ubiquitous flavin-dependent enzymes that commonly facilitate redox chemistry such as the oxygenation of organic substrates. Here we employ O_2-pressurized X-ray crystallography and quantum mechanical calculations to reveal how the precise positioning of O_2 within a flavoenzyme's active site enables the regiospecific formation of a covalent flavin–oxygen adduct and oxygenating species (i.e., the flavin-N5-oxide) by mimicking a critical transition state. This study unambiguously demonstrates how enzymes may control the O_2 functionalization of an organic cofactor as prerequisite for oxidative catalysis. Our work thus illustrates how O_2 reactivity can be harnessed in an enzymatic environment and provides crucial knowledge for future rational design of O_2-reactive enzymes.

monooxygenase | EncM | FAD | flavin-N5-oxide | bioengineering

Small gaseous molecules such as O_2 are essential for numerous enzymatic reactions in nature with significant potential for biomedical application (1). However, the structural and biochemical requirements for O_2 enzyme catalysis remain largely elusive (1–10), in particular for the highly versatile reaction of enzyme-bound reduced flavin (Fl_{red}) with hydrophobic O_2 (2, 3, 10–12). Flavoenzymes mainly mediate redox reactions (13) while nonredox chemistry (14) and covalent catalysis (15) become increasingly recognized. This extraordinary chemical prowess of the flavin cofactor is a result of the isoalloxazine ring system and the N5–C4a locus in particular, which allows the uptake of one or two electrons in its oxidized resting state (Fl_{ox}), thus producing radical flavin semiquinone (Fl_{SQ}) and Fl_{red}, respectively. In addition, covalent intermediates with N5 or C4a can be formed, e.g., with organic substrates or O_2. Flavin functionalization via formation of covalent oxygen adducts is crucial for oxygenase activity and achieved through reaction of Fl_{red} with O_2, most likely giving rise to a short-lived Fl_{SQ} and superoxide caged radical pair before generating a transient flavin-C4a-hydroperoxide (Fl_{C4aOOH}) (16–18) or the stable flavin-N5-oxide (Fl_{N5O}) (19–22) oxygenating species (Fig. 1). The versatile reactions of O_2 with enzyme-bound flavins are assumed to be fine-tuned by the immediate chemical environment, i.e., accessibility for O_2, electrostatics, and the ability of the flavin to assume distorted conformations (1–3, 11). For example, a putative O_2 cavity has been proposed to ensure the "face-on" approach of O_2 to C4a of the flavin cofactor in line with the mechanistic requirements for Fl_{C4aOOH} formation (2, 23, 24). However, despite these significant advances in our understanding of flavin biochemistry, direct evidence of the precise binding and interaction of O_2 with a flavoprotein has not been furnished, and the exact active-site structural features that govern formation of flavin oxygenating species remain elusive (1, 2). The surprising discovery of the novel Fl_{N5O} oxygenating species in the noncanonical bacterial flavin-dependent monooxygenase EncM involved in polyketide biosynthesis (20, 21) and additional

flavoenzymes (25, 26) has further convoluted the research field. Hence, it remains unclear how O_2 reactivity can be controlled within flavoenzyme active sites to ensure the regiospecific radical coupling at C4a or N5 and thereby steer the formation of Fl_{C4aOOH} or Fl_{N5O}, respectively. In this work, we set out to investigate the mechanistic and structural basis for the formation of covalent flavin–oxygen adducts by using EncM as a model system.

Results

EncM Features a Distinct Putative O_2 Pocket at the *re*-Side of the Flavin. As our working hypothesis, we propose that the enzymatic synthesis of the Fl_{N5O} involves a direct radical coupling mechanism at N5 affording Fl_{N5OOH} (Fig. 1B) (20). Fl_{N5O} formation presumably necessitates rigorous control of the reaction of flavin with O_2 and the postulated transient protonated superoxide species. When we inspected the internal surface of the flavin surroundings in EncM (21), a distinct amphiphilic cavity became apparent at the *re*-side of the covalently bound flavin cofactor (*SI Appendix*, Fig. S1), which may be suitable to accommodate the hydrophobic O_2 as well as the hydrophilic protonated superoxide. Indeed, an O_2 pocket at this location appears likely based on in silico docking analysis (*SI Appendix*, Fig. S2). Notably, the polyketide substrate is positioned on the opposite *si*-side of the cofactor (21), suggesting separate active sites for O_2 activation and substrate oxidation in EncM, in line with structurally related flavoenzymes (4).

Significance

Vitamins are often precursors for the biosynthesis of organic enzyme cofactors, as exemplified by the ubiquitous vitamin B2-derived flavins. Enzymes employ flavins, e.g., to oxygenate organic substrates with the help of covalent flavin–oxygen adducts that serve as oxygenating species. However, details of the preceding reaction of O_2 with the reduced flavin cofactor that gives rise to these oxygenating species remain scarce. We have now shown how a flavoenzyme interacts with O_2 and controls the formation of an oxygenating species as key to oxidative catalysis. This knowledge will be useful for the bioengineering of flavoenzymes and fine-tuning of their O_2 reactivity.

Fig. 1. Flavin oxygenating species and their formation. (*A*) Structures and simplified routes for enzymatic formation of Fl_{C4aOOH} and Fl_{N5ox}. (*B*) Proposed detailed pathway for EncM-Fl_{N5ox} formation. Fl_{red} reacts with O_2 by H-transfer, forming anionic Fl_{SQ} [with high spin density at N5 (27, 28)] and protonated superoxide. Spin inversion and radical coupling then gives rise to transient Fl_{N5OOH}, followed by elimination of elimination of OH^-, thus producing stable Fl_{N5ox} (two resonance forms are shown).

Dioxygen-Pressurized X-Ray Crystallography Exposes EncM's Dioxygen Reaction Site. We next attempted to acquire direct experimental evidence for the proposed O_2 pocket. For that, we employed O_2-pressurized X-ray crystallography (29) and incubated EncM crystals with 5, 10, or 15 bars of O_2 gas in a modified Xe-pressurization cell (Xcell; Oxford Cryosystems) for 10 min, before pressure release and instantaneous freezing of the crystals in liquid nitrogen. We furthermore prepared crystals under atmospheric partial O_2 pressure (0.21 bar) and, as a control, under anaerobic argon atmosphere. In total, at least eight individual EncM active sites were analyzed for each condition. All analyzed crystals diffracted

between 1.4 to 3.0 Å [*SI Appendix*, Table S1, includes refinement statistics and Protein Data Bank (PDB) ID codes of all protein structures solved in this work]. For improved accuracy and reliability of our omit electron density maps around the putative O_2 pocket, we used phenix.polder (30).

Indeed, we observed highly significant electron densities in the cavities at the *re*-side of the flavin for aerobic crystals at all examined pressure levels, indicating the presence of O_2. This went along with the concomitant increase in occupancy and signal intensity for crystals exposed to 0.21, 5, 10, and 15 bars of O_2 pressure, respectively (Fig. 2 *A*–*C*). The omit maps furthermore enabled precise positioning of the O_2 molecule in the ovoid-shaped electron density and thus determination of the exact geometry and arrangement with respect to the flavin cofactor. Accordingly, the nearest oxygen atom (O1) of O_2 is positioned directly in front of N5 at a distance of 2.7 Å and at an angle of 118° between the N5–N10 axis and N5–O1. O1 is furthermore in hydrogen-bonding distance of the backbone amide groups of Val136 (2.5 Å) and Val135 (2.6 Å), whereas the second oxygen atom (O2) is 3.0 Å away from N5 and close to the T139 side chain (2.5 Å), as well as the main-chain carbonyl group of Val136 (3.2 Å; Fig. 3 *A* and *B*). The well-ordered electron densities furthermore imply a small degree of motional freedom for O_2 that is in direct contact with the flavin cofactor and thus poised to participate in short-range electron transfer, which has been previously suggested to be a possible prerequisite for the formation of covalent flavin–oxygen adducts by monooxygenases (1). Interestingly, a second O_2 site was identified in the elongated substrate-binding tunnel of EncM, approximately halfway between the tunnel entrance and the flavin, which may facilitate channeling of O_2 into EncM (*SI Appendix*, Fig. S3). Importantly, the polder omit maps calculated from the anaerobically grown control crystals of EncM revealed no significant electron density beyond background noise in the O_2 cavity at contour levels >3σ. To ensure that the anaerobic conditions did not otherwise affect EncM crystallization, we pressurized anaerobically prepared crystals with 15 bars of O_2 as an additional control experiment and then observed clear electron density in the cavity (*SI Appendix*, Fig. S4). Interestingly, O_2 binding did not result in evident spectral changes of the flavin cofactor, as verified by UV-visible

Fig. 2. O_2-pressurized X-ray crystallographic data of EncM. Shown are the O2 reaction sites of EncM WT crystals under anaerobic (0 bar O_2, *A*), aerobic (0.21 bar partial O_2 pressure, i.e., atmospheric level, *B*), and O_2 pressurized (15 bar O_2, *C*) conditions (pressure levels of 5 and 10 bars of O_2 are not shown). All shown polder omit maps (F_o–F_c) of EncM·O_2 complexes were contoured at 5σ above the mean (O_2 molecules not included in the refinement). (*D*) Occupancy of O_2 atoms in the O_2 pockets of the EncM crystal structures (WT and variant L144M; see also Fig. 3*C*) at various O_2 pressure levels (error bars represent the SD for $n = 8$ individual EncM O_2 pockets for each condition). (*E*) Representation of the internal surface of the flavin surroundings in O_2-pressurized (15 bars) EncM WT showing O_2 bound in the cavity (O_2 was positioned as ball-and-stick model in the extra density, but not included in the refinement).
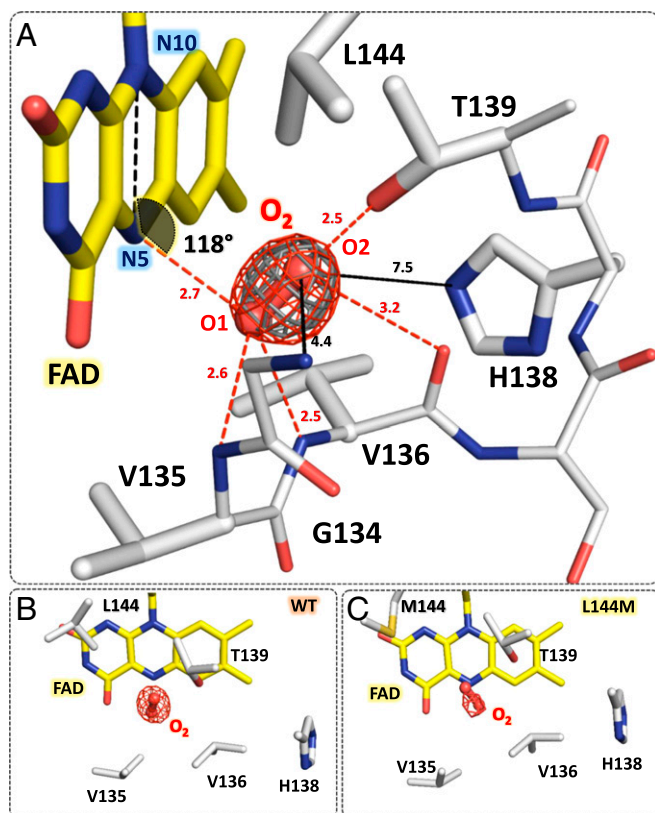
Saleem-Batcha et al.

Fig. 3. Detailed view of the amphiphilic O_2 reaction site of EncM and critical amino acid residues. All shown polder omit electron density maps for O_2 (red mesh) were contoured at 5σ above the mean (O_2 was positioned as ball-and-stick model in the extra densities, but not included in the refinement). The refined 2Fo–Fc electron density map (gray mesh) in A was contoured at 1.5σ above the mean (O_2 was positioned as ball-and-stick model in the extra density and included in the refinement). (A) EncM WT O_2 reaction site at 15 bars of O_2 pressure. Distances <3.5 Å likely relevant for H-bonding interactions with the transient protonated superoxide radical are indicated with red dotted lines. Distances >3.5 Å are drawn as black dotted lines. (B) Alternate view of 15 bars O_2-pressurized EncM WT illustrating how the O_2 molecule is positioned in front of N5 of the flavin isoalloxazine ring. (C) Crystal structure of the EncML144M variant pressurized at 15 bar of O_2 showing significantly weaker electron density and altered O_2 orientation.

(UV-vis) spectroscopy of anaerobic and aerobic EncM (*SI Appendix,* Fig. S5).

Xenon and Halide Ions Do Not Bind in the Vicinity of EncM's Flavin. In the past, indirect evidence of O_2 binding sites was commonly furnished with X-ray crystallography with the use of chemical O_2 surrogates such as hydrophobic xenon gas, which has adequately similar size and chemical properties (29, 31–33). However, xenon seems unsuitable for O_2 reaction sites, i.e., sites that not only bind O_2, but, e.g., also promote formation of superoxide. Consequently, chloride and bromide were used as superoxide surrogates and shown to bind to proposed O_2 reaction sites in various redox enzymes (4, 29, 31, 34–36), including flavin-dependent oxidases (4, 35). We thus tested whether xenon, bromide, or chloride can occupy the O_2 cavity of EncM via X-ray crystallography (by applying xenon overpressure or by soaking of anaerobically grown crystals with 1.5 M sodium bromide or 1.5 M potassium chloride, respectively) as well as chloride titration combined with UV-vis spectroscopy. Analysis of the crystals indeed revealed distinct xenon and bromide binding sites (bromide site 1 was identical to the second O_2 site in the substrate-binding tunnel of EncM; *SI Appendix,* Fig. S6 *A and B*), yet no significant electron densities were observed in the direct vicinity of the flavin cofactor. Similarly,

chloride binding could not be observed close to the EncM's flavin (*SI Appendix,* Fig. S6C), suggesting a high degree of specificity for O_2/superoxide and furthermore bringing into question the reliability of these surrogates for the detection of O_2 binding and reaction sites in other enzymes. Notably, the lack of halide anion binding in EncM's O_2 reaction site may also reflect an adaptation to the enzymatic interaction with uncharged protonated superoxide as opposed to the superoxide anion.

Alteration of EncM's Dioxygen Reactivity via Mutagenesis of the Dioxygen Pocket. To further investigate the importance of the identified O_2 reaction site for EncM-Fl_{N5O} formation and oxygenase functionality, we targeted and modified the geometry of the pocket via site-directed mutagenesis. Accordingly, small hydrophobic amino acid residues were replaced with bulky hydrophobic ones (e.g., V135M and L144M) to interfere with access of O_2 to the reaction site. We also introduced an isosteric mutation (T139V) to remove a potential hydrogen-bonding partner for the proposed transiently formed superoxide intermediate. In addition, further single and double mutants on residues forming the O_2 pocket were generated (listed in *SI Appendix,* Table S2), which, however, led to unstable protein. The structures of all stable variants were solved via X-ray crystallography, showing conservation of the protein fold and high overall similarity with the WT (Δrmsd values <0.5 Å). Typically, virtually all of the EncM WT harbors Fl_{N5O} when isolated from the heterologous host (21). In contrast, all investigated EncM variants, including T139V, V135M, L144M, and H138T, contained mostly Fl_{ox} and only minor amounts of Fl_{N5O} upon isolation, as indicated by the enzyme color and further verified by UV-vis spectroscopy and MS (*SI Appendix,* Figs. S7 and S8). This suggests that Fl_{N5O} formation is less efficient in these variants, presumably by affecting the binding and spatial positioning of O_2 or, in the case of T139V, the interaction with superoxide. To confirm this, we employed O_2-pressurized X-ray crystallography on the L144M variant of EncM as an example. Indeed, even at 15 bars of O_2, low occupancy, weak electron density, and altered spatial arrangement of O_2 compared with EncM WT was observed (Figs. 2D and 3C).

Fl_{N5O} Formation Is Significantly Impeded in the EncM Variants. Next, we directly measured the O_2 consumption and H_2O_2 production of EncM WT and variants by using an O_2 optode to gain more insight into the O_2 reactivity and proficiency to form Fl_{N5O}. For that, the flavin cofactors of EncM WT and variants were first converted into Fl_{ox} by reduction with dithionite in an anaerobic chamber, followed by reoxidation with the chemical oxidant dichloroindophenol (21). The absence of O_2 thereby ensured complete oxidation to the Fl_{ox} redox state instead of the Fl_{N5O} or mixtures thereof. Next, we quantified the amount of O_2 required to fully regenerate Fl_{N5O}. For that, NADPH was added under aerobic conditions to reduce EncM-Fl_{ox} to Fl_{red}, which subsequently reacts with O_2 and forms Fl_{N5O} [NADPH rapidly reduces EncM-Fl_{ox}, but reacts very poorly with EncM-Fl_{N5O} (20)]. As anticipated, Fl_{N5O} formation in EncM WT required approximately 1 mol of O_2 per mole of Fl_{red}, confirming that EncM-Fl_{red} oxidation with O_2 reliably affords EncM-Fl_{N5O}. In contrast, the EncM variants T139V, L144M, and V135M consumed 18, 16, and 17 mol O_2 per mole Fl_{red}, respectively. In addition, H_2O_2 was produced by these variants (*SI Appendix,* Fig. S9), showing that Fl_{N5O} formation is significantly affected and that EncM is converted from an oxygenase into a (partial) H_2O_2-producing oxidase when amino acid residues at the *re*-side of the cofactor are replaced, as opposed to mutations conducted at the *si*-side (20, 21).

EncM-Fl_{red} May Bind O_2 Before Forming EncM-Fl_{N5O}. To further investigate the kinetic mechanism of this reaction, the O_2-concentration dependence of EncM-Fl_{red} oxidation was examined via stopped-flow spectroscopy. O_2 oxidizes EncM-Fl_{red} directly into EncM-Fl_{N5O} without detectable formation of any intermediates (20) and occurred in two phases with similar amplitudes, potentially indicating asymmetry in the two active sites of the EncM

homodimer (*SI Appendix*, Fig. S10). Remarkably, the observed rate constants (k_{obs}) for both phases increased hyperbolically with the O_2 concentration, reaching saturating values at limiting O_2 concentrations. This pattern is consistent with a two-step kinetic mechanism whereby O_2 first binds to EncM-Fl_{red} before forming EncM-Fl_{N5O} and qualitatively corroborates the O_2 observed near N5 in our O_2-pressurized crystals of EncM. The K_d values obtained from the fit of k_{obs} against O_2 concentration are 290 and 630 μM for the first and second phases, respectively, making the rate of Fl_{N5O} formation highly tunable with respect to the O_2 concentration. Consequently, in line with our X-ray crystallographic data, EncM may truly bind O_2 in contrast to the rapid consumption by common flavin oxidases/oxygenases with bimolecular rate constants as high as 10^6 $M^{-1}\cdot s^{-1}$ [referred to in a previous work as the "O_2-binding vs. O_2-consuming paradigm" (1)]. This furthermore suggests that enzymatic Fl_{N5O} formation necessitates meticulous control of the reaction between Fl_{red} and O_2, as further corroborated by our mutational studies showing that minor changes of the geometry (e.g., L144M) or polarity (isosteric mutation T139V) of the distinct cavity at the *re*-side of the flavin result in drastic changes in O_2 reactivity. Consistently, stopped-flow measurements of EncM-Fl_{red} T139V showed that k_{obs} increased linearly with the O_2 concentration instead of the hyperbolic dependence of EncM-Fl_{red} WT (*SI Appendix*, Fig. S10). This is consistent with EncM T139V acting as an oxidase that reacts directly with O_2 to make H_2O_2 or superoxide instead of binding O_2.

Thermochemistry Calculations Support Fl_{N5O} Formation via Fl_{N5OOH}.
To provide a rationale for how flavoproteins are able to steer the regiospecific radical coupling with the superoxide at N5 and furthermore substantiate a transient pyramidal *sp3* hybridized Fl_{N5OOH} intermediate en route to Fl_{N5O} formation, we performed quantum mechanical calculations on intermediates and transition states for the reaction pathway using UB3LYP density functional theory (Fig. 4; see *SI Appendix* for more details). In the absence of an enzyme, the calculations predicted similar activation energy barriers for bond formation between oxygen and C4a to form Fl_{C4aOOH} (12.5 kcal/mol) and between oxygen

and N5 to form Fl_{N5OOH} (12.0 kcal/mol), revealing that both reactions are energetically plausible and suggesting that, aside from the protonation state of the Fl_{SQ}, the positioning of O_2 with respect to the flavin cofactor will ultimately determine whether reaction at C4a or N5 has a lower activation barrier in the active site of a flavin-dependent enzyme. Along the Fl_{N5O} pathway, the critical transition state leading to the formation of the Fl_{N5OOH} (Fig. 4, *Inset*) closely resembles the EncM binding mode of O_2 (Fig. 3 *A* and *B*), with a strikingly similar arrangement of the oxygen atoms with respect to the flavin cofactor, suggesting that the active site is preorganized to lower the energy of this transition state and accelerate the formation of Fl_{N5OOH} over the formation of Fl_{C4aOOH}. The transition state for the first step involving hydrogen abstraction from Fl_{red} by O_2 actually lies below the separated reactants as a result of the formation of a stable complex between the reactants. The transition state for the final step involving loss of hydroxide is rate-determining in the absence of an enzyme, suggesting that another key role of EncM is the stabilization of the hydroxide leaving group through hydrogen bonding to the T139 side chain or backbone amides, as corroborated by our structural data showing that the distal O2 atom of the O_2 molecule is oriented toward T139 at a distance of only 2.5 Å (Fig. 3*A*). These computations confirm the energetic feasibility of Fl_{N5O} formation via Fl_{N5OOH} and suggest that the enzyme active site is optimized to lower the activation barriers for bond formation at N5 and subsequent hydroxide elimination to generate the Fl_{N5O}.

Discussion

The pathway for generation of the Fl_{N5O} is reminiscent of the proposed Fl_{C4aOOH} formation by common flavin oxygenases, as O_2 also approaches the flavin "face-on" in EncM. The absence of a positive charge (commonly used to facilitate formation of superoxide anions in proteins) (10, 11, 35), together with the lack of halide binding in EncM, support the proposed hydrogen transfer from EncM-Fl_{red} to O_2 that yields uncharged protonated superoxide and thereby circumvents electrostatic repulsion
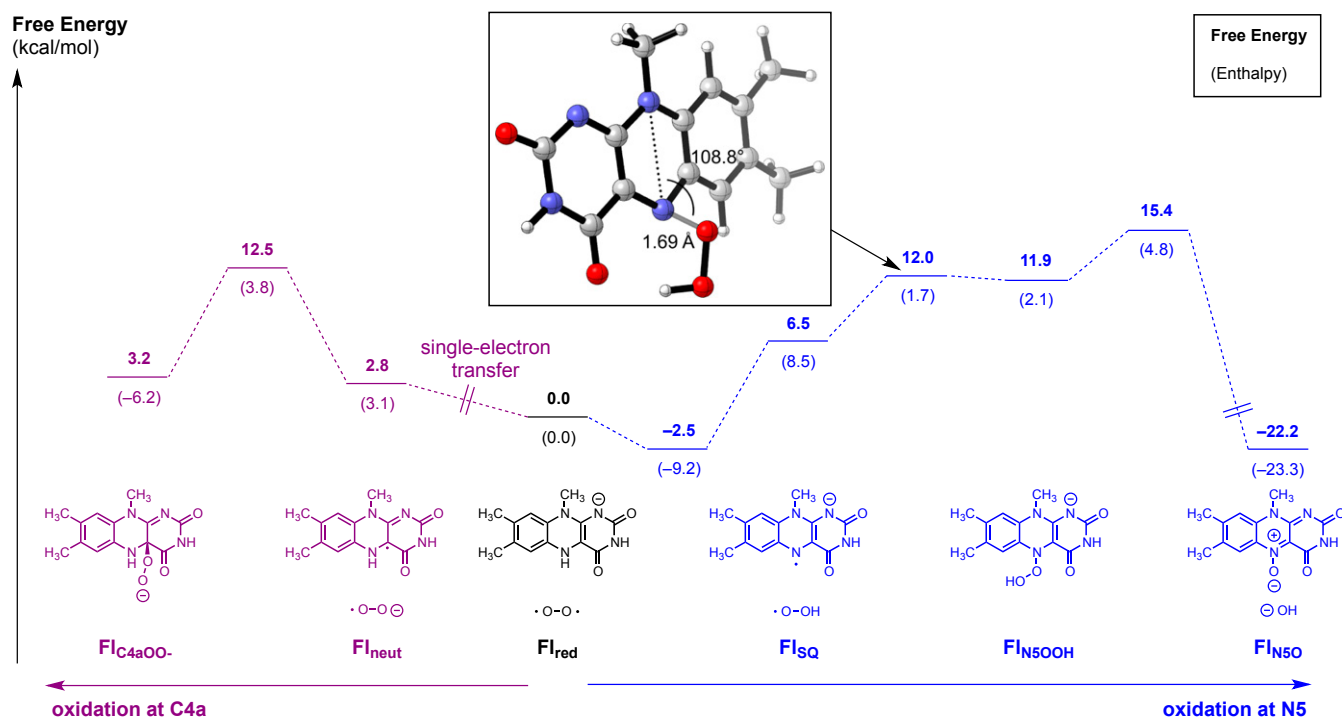

Fig. 4. Free energies (enthalpy values shown in brackets below) for the reactions between Fl_{red} and O_2 to form $Fl_{C4aCOO-}$ (purple pathway) or Fl_{N5O} (blue pathway), confirming that the pathway for Fl_{N5O} formation is kinetically and thermodynamically feasible. Fl_{neut}, neutral Fl_{SQ}. (*Inset*) Calculated transition state for the formation of Fl_{N5OOH}, which closely resembles the binding mode of O_2 in the EncM active site. Energies with UB3LYP-D3(BJ)/6–311++G(2d,2p)/IEFPCM (H_2O).

between the anionic SQ and the superoxide anion. EncM is likely optimized to binding of protonated superoxide instead of O_2, as enzymes are commonly shaped by evolution to efficiently interact with transition states rather than the (co)substrate itself. The retention of superoxide is furthermore critical for any O_2-reactive flavoprotein, as its escape would be detrimental to the cell as a result of its reactivity and toxicity and, in the case of EncM, would also prevent Fl_{N5O} formation. The amphiphilic nature of the O_2 reaction site in EncM may therefore reflect a trade-off between proper positioning of hydrophobic O_2 and retention of the transiently formed hydrophilic superoxide radical to satisfy the mechanistic demands for Fl_{N5O} formation. The O_2 cavity of EncM enables the efficient radical coupling at N5 while avoiding deleterious side reactions such as the production of H_2O_2 or the release of superoxide, a first among O_2-reactive flavoproteins. The separate active sites in EncM presumably allow the simultaneous binding of the polyketide substrate and O_2 on the *si*-side and *re*-side of the flavin cofactor, respectively. As a consequence, when the Fl_{N5O} has fully oxidized the substrate and is converted to Fl_{red}, a prepositioned O_2 molecule may ensure Fl_{N5O} formation and prevent uncontrolled flavin reoxidation and production of reactive oxygen species. A distinct O_2 reaction site can also be rationalized from a thermodynamic point of view, as binding of the sizeable substrate desolvates the *si*-side of EncM's flavin and therefore lowers the polarity, thereby impeding superoxide formation at this location, as similarly reported for other flavoproteins (12). Hence, the presence of a spatially separated O_2 reaction site in EncM most likely renders the formation of protonated superoxide thermodynamically favorable.

In summary, our data have imparted detailed insight into the interaction of O_2 with an enzyme as prerequisite for flavin cofactor functionalization and generation of the catalytically active oxygenating species. Our analyses revealed considerable structural constraints with respect to O_2 positioning, thereby explaining why Fl_{N5O} is not formed by O_2 and Fl_{red} in solution, but is only achievable in a highly adapted anisotropic active site of an enzyme. The presented methodology here may be applicable to other oxidases and oxygenases and ultimately allow a more comprehensive picture of the remarkable interplay between enzymes and O_2. This work sets the stage for future bioengineering of O_2-reactive enzymes such as the de novo design or redesign of flavin oxygenases and provides crucial missing puzzle pieces for the question how enzymes control the reactions with gaseous molecules such as O_2.

Materials and Methods

All reagents were purchased commercially and used without further purification.

Computational Docking. O_2-binding mode in EncM WT and its variants was screened by using the structure-based virtual screening and automatic docking tool iGEMDOCK (37). Covalently linked FAD molecules were considered for O_2 docking calculations. Fitness score is the total energy of a predicted O_2 docking pose in the O_2 reaction site.

Mutagenesis, Expression, and Protein Production. Mutations were introduced into the pHIS8-*encM* vector (38), which contained the *encM* gene, using the QuikChange mutagenesis protocol from Stratagene (Agilent) and HPLC-purified primers (*SI Appendix*) from Sigma-Aldrich. Genes were sequenced (GATC Biotech) following Q5 polymerase amplification (NEB) to confirm the mutations and then transformed and expressed in *Escherichia coli* BL21(DE3) cells (Novagen). Cells were harvested by centrifugation, lysed by using an Ultrasonifier, and centrifuged at 18,000 × *g* (relative centrifugal force) for 20 min. The protein in the supernatant was further purified according to standard procedures as described before (21).

Spectroscopic Analyses. UV-vis absorption spectra were recorded as described previously (21). Stopped-flow experiments were performed by using a Hi-Tech Scientific KinetAsyst SF-61 DX2 stopped-flow spectrophotometer at 4 °C in 0.1 M Tris·H_2SO_4, pH 7.5, 10% glycerol. Enzyme solutions were made anaerobic in glass tonometers by repeated cycles of vacuum and equilibration with anaerobic argon. The enzyme-bound flavin was reduced anaerobically in the tonometer by titrating with dithionite. Buffers with various oxygen concentrations were prepared by bubbling buffers with O_2/N_2 gas

mixtures. A total of 18 μM (after mixing) EncM-Fl_{red} was mixed with various O_2 buffers (31–615 μM after mixing), and the reaction was monitored by diode array. Reaction traces at 450 nm were fit to a double exponential in KaleidaGraph. The two observed rate constants for the two exponentials increased hyperbolically with the O_2 concentration. Plots of k_{obs} against O_2 concentration were fit to a hyperbola in KaleidaGraph.

Oxygen Optode Assays. Kinetic measurements of the O_2 consumption in enzymatic assays (150 μL) were conducted by using a MICROX TX3 fiberoptic oxygen meter (oxygen optode; PreSens) calibrated at 23 °C with air-saturated buffer (50 mM Tris·HCl, pH 7.7, and 300 mM NaCl) as 100% O_2 (corresponding to 0.269 mM O_2) and freshly prepared 100 mM dithionite in the same buffer as 0% of O_2. The assay contained 15 μM of EncM WT ± 20 nM catalase and 5 μM of EncM variants ± 20 nM catalase. The assay was started by the addition of 4 mM NADPH.

Crystallization, Halide Ion Derivatization, and Gas (Xe and O_2) Pressurized Crystallography. Well-diffracting polygonal-shaped crystals of EncM WT and variants under aerobic and/or anaerobic conditions were grown within 4–7 d in sitting drops as described earlier (21). O_2 or xenon derivatives were produced at room temperature by pressurizing crystals of EncM WT or EncM variants by using a pressurization cell (Xcell; Oxford Cryosystems) at the PXI-X06SA and PXII-X10SA beamlines (SLS). The cell initially developed for xenon gas was adapted for the use of pure O_2 gas. For O_2 gas pressurization (29), a crystal was mounted in a nylon loop from the mother liquor, dipped through cryoprotectant (25% vol/vol glycerol), and placed in the pressure vessel. Following incubation (10 min), the pressure was released (10 s) and the crystal was flash-frozen by being plunged into liquid nitrogen. Multiple pressure levels (0.5–1.5 MPa) were tested. Pressure levels greater than 1.5 MPa damaged the crystals. For chloride and bromide derivatization, EncM was crystallized in presence of 2 M sodium chloride under anaerobic conditions, and anaerobically grown crystals were soaked in crystallization solution containing 1.5 M sodium bromide or 1.5 M potassium chloride. Several datasets of each pressure levels, cocrystals, soaks, and variants were individually screened for diffraction. In total, 36 complete datasets of crystals (12 datasets in triplicate) were analyzed, and 12 were submitted to PDB. Refinement statistics and PDB ID codes are provided in *SI Appendix*, Table S1.

X-Ray Diffraction and Structure Determination. High-quality X-ray diffraction datasets were obtained with resolutions as high as 1.4 Å at the PXI-X06SA beamline (SLS) at a wavelength of 1.0 Å by using an EIGER 16M X (133 Hz; Dectris) detector. Intensity data were collected (φ scans of 0.1° over 360°) to a resolution of 1.4 Å from individual single crystals. Data processing and scaling were performed in XDS (39) and SCALA (40), respectively. The data collection and refinement statistics are given in *SI Appendix*, Table S1. The structure was determined by molecular replacement by using PHASER (41), and initially refined in REFMAC (42). Final refinement and manual rebuilding were performed by using phenix.refine as implemented in PHENIX (43) and COOT (44), respectively. Solvent molecules were placed automatically by using PHENIX, and refinement was continued until no features remained in the Fo − Fc difference maps. For omit map calculations, the Polder OMIT maps tool (30) was used. MolProbity (45) was used to check the structure quality before deposition in PDB.

Liquid Chromatography/MS Analysis. Proteinase K-digested EncM WT and EncM variants were subjected to high-resolution electrospray ionization liquid chromatography/MS as described earlier (20) for detection of structure of the flavinylated hexapeptide GGGH$_{78}$[−Fl_{N5O}]SM with a calculated MH$^+$ of 1,344.35 and GGGH$_{78}$[−Fl_{ox}]SM with a calculated MH$^+$ of 1,328.355. The respective oxidation states of the detected peptide-bound flavin cofactors are estimated based on the ratio of Fl_{N5O} to Fl_{ox}.

Computational Methods. Conformational searches of all intermediates involving the flavin cofactor were performed by using the Schrödinger MacroModel (46) software package to identify low-energy conformers for quantum mechanical calculations; reported quantum mechanical energies and geometries are for the lowest-energy conformer. All quantum mechanical calculations were performed by using the Gaussian 09 (47) software package. Structures were optimized at the UB3LYP (48, 49)/6−31+G(d) level of theory using the integral-equation-formalism polarizable continuum model (IEFPCM) (50–52) solvent model for water, which was chosen to mimic the role of the enzyme active site in stabilizing charges; frequency calculations were used to confirm the presence of local minima (i.e., no imaginary frequencies) and transition states (i.e., one imaginary frequency) and to calculate free energies at 298 K. To obtain more accurate energetics, single-point energy calculations were performed on the

1. Baron R, McCammon JA, Mattevi A (2009) The oxygen-binding vs. oxygen-consuming paradigm in biocatalysis: Structural biology and biomolecular simulation. *Curr Opin Struct Biol* 19:672–679.
2. Chaiyen P, Fraaije MW, Mattevi A (2012) The enigmatic reaction of flavins with oxygen. *Trends Biochem Sci* 37:373–380.
3. McDonald CA, Fagan RL, Collard F, Monnier VM, Palfey BA (2011) Oxygen reactivity in flavoenzymes: Context matters. *J Am Chem Soc* 133:16809–16811.
4. Zafred D, et al. (2015) Rationally engineered flavin-dependent oxidase reveals steric control of dioxygen reduction. *FEBS J* 282:3060–3074.
5. Orville AM, Lountos GT, Finnegan S, Gadda G, Prabhakar R (2009) Crystallographic, spectroscopic, and computational analysis of a flavin C4a-oxygen adduct in choline oxidase. *Biochemistry* 48:720–728.
6. Baron R, et al. (2009) Multiple pathways guide oxygen diffusion into flavoenzyme active sites. *Proc Natl Acad Sci USA* 106:10603–10608.
7. Cohen J, Schulten K (2007) O2 migration pathways are not conserved across proteins of a similar fold. *Biophys J* 93:3591–3600.
8. Saam J, Ivanov I, Walther M, Holzhütter HG, Kuhn H (2007) Molecular dioxygen enters the active site of 12/15-lipoxygenase via dynamic oxygen access channels. *Proc Natl Acad Sci USA* 104:13319–13324.
9. Johnson BJ, et al. (2007) Exploring molecular oxygen pathways in Hansenula polymorpha copper-containing amine oxidase. *J Biol Chem* 282:17767–17776.
10. Klinman JP (2007) How do enzymes activate oxygen without inactivating themselves? *Acc Chem Res* 40:325–333.
11. Mattevi A (2006) To be or not to be an oxidase: Challenging the oxygen reactivity of flavoenzymes. *Trends Biochem Sci* 31:276–283.
12. Wang R, Thorpe C (1991) Reactivity of medium-chain acyl-CoA dehydrogenase toward molecular oxygen. *Biochemistry* 30:7895–7901.
13. Walsh CT, Wencewicz TA (2013) Flavoenzymes: Versatile catalysts in biosynthetic pathways. *Nat Prod Rep* 30:175–200.
14. Sobrado P, Tanner JJ (2017) Multiple functionalities of reduced flavin in the nonredox reaction catalyzed by UDP-galactopyranose mutase. *Arch Biochem Biophys* 632:59–65.
15. Piano V, Palfey BA, Mattevi A (2017) Flavins as covalent catalysts: New mechanisms emerge. *Trends Biochem Sci* 42:457–469.
16. Palfey BA, McDonald CA (2010) Control of catalysis in flavin-dependent monooxygenases. *Arch Biochem Biophys* 493:26–36.
17. Massey V (1994) Activation of molecular oxygen by flavins and flavoproteins. *J Biol Chem* 269:22459–22462.
18. Huijbers MM, Montersino S, Westphal AH, Tischler D, van Berkel WJ (2014) Flavin dependent monooxygenases. *Arch Biochem Biophys* 544:2–17.
19. Teufel R, Agarwal V, Moore BS (2016) Unusual flavoenzyme catalysis in marine bacteria. *Curr Opin Chem Biol* 31:31–39.
20. Teufel R, et al. (2015) Biochemical establishment and characterization of EncM's flavin-N5-oxide cofactor. *J Am Chem Soc* 137:8078–8085.
21. Teufel R, et al. (2013) Flavin-mediated dual oxidation controls an enzymatic Favorskii-type rearrangement. *Nature* 503:552–556.
22. Teufel R (2017) Flavin-catalyzed redox tailoring reactions in natural product biosynthesis. *Arch Biochem Biophys* 632:20–27.
23. Schreuder HA, Hol WGJ, Drenth J (1990) Analysis of the active site of the flavoprotein p-hydroxybenzoate hydroxylase and some ideas with respect to its reaction mechanism. *Biochemistry* 29:3101–3108.
24. Alfieri A, et al. (2007) Structure of the monooxygenase component of a two-component flavoprotein monooxygenase. *Proc Natl Acad Sci USA* 104:1177–1182.
25. Adak S, Begley TP (2017) RutA-catalyzed oxidative cleavage of the uracil amide involves formation of aflavin-N5-oxide. *Biochemistry* 56:3708–3709.
26. Adak S, Begley TP (2016) Dibenzothiophene catabolism proceeds via aflavin-N5-oxide intermediate. *J Am Chem Soc* 138:6424–6426.
27. Massey V, Hemmerich P (1980) Active-site probes of flavoproteins. *Biochem Soc Trans* 8:246–257.
28. Barquera B, et al. (2003) X- and W-band EPR and Q-band ENDOR studies of the flavin radical in the Na+ -translocating NADH:quinone oxidoreductase from *Vibrio cholerae*. *J Am Chem Soc* 125:265–275.
29. Colloc'h N, et al. (2008) Oxygen pressurized x-ray crystallography: Probing the dioxygen binding site in cofactor lessurate oxidase and implications for its catalytic mechanism. *Biophys J* 95:2415–2422.
30. Liebschner D, et al. (2017) Polder maps: Improving OMIT maps by excluding bulk solvent. *Acta Crystallogr D Struct Biol* 73:148–157.
31. Duff AP, et al. (2004) Using xenon as a probe for dioxygen-binding sites in copper amine oxidases. *J Mol Biol* 344:599–607.
32. Tilton RF, Jr, Kuntz ID, Jr, Petsko GA (1984) Cavities in proteins: Structure of a metmyoglobin-xenon complex solved to 1.9 A. *Biochemistry* 23:2849–2857.
33. Hiromoto T, Fujiwara S, Hosokawa K, Yamaguchi H (2006) Crystal structure of 3-hydroxybenzoate hydroxylase from Comamonas testosteroni has a large tunnel for substrate and oxygen access to the active site. *J Mol Biol* 364:878–896.
34. Roeser D, Schmidt B, Preusser-Kunze A, Rudolph MG (2007) Probing the oxygen-binding site of the human formylglycine-generating enzyme using halide ions. *Acta Crystallogr D Biol Crystallogr* 63:621–627.
35. Kommoju PR, Chen ZW, Bruckner RC, Mathews FS, Jorns MS (2011) Probing oxygen activation sites in two flavoprotein oxidases using chloride as an oxygen surrogate. *Biochemistry* 50:5521–5534.
36. Gabison L, et al. (2010) Near-atomic resolution structures of urate oxidase complexed with its substrate and analogues: The protonation state of the ligand. *Acta Crystallogr D Biol Crystallogr* 66:714–724.
37. Hsu KC, Chen YF, Lin SR, Yang JM (2011) iGEMDOCK: A graphical environment of enhancing GEMDOCK using pharmacological interactions and post-screening analysis. *BMC Bioinformatics* 12:S33.
38. Jez JM, Ferrer JL, Bowman ME, Dixon RA, Noel JP (2000) Dissection of malonyl-coenzyme A decarboxylation from polyketide formation in the reaction mechanism of a plant polyketide synthase. *Biochemistry* 39:890–902.
39. Kabsch W (2010) Xds. *Acta Crystallogr D Biol Crystallogr* 66:125–132.
40. Evans P (2006) Scaling and assessment of data quality. *Acta Crystallogr D Biol Crystallogr* 62:72–82.
41. McCoy AJ, et al. (2007) Phaser crystallographic software. *J Appl Cryst* 40:658–674.
42. Murshudov GN, Vagin AA, Dodson EJ (1997) Refinement of macromolecular structures by the maximum-likelihood method. *Acta Crystallogr D Biol Crystallogr* 53:240–255.
43. Adams PD, et al. (2010) PHENIX: A comprehensive Python-based system for macromolecular structure solution. *Acta Crystallogr D Biol Crystallogr* 66:213–221.
44. Emsley P, Cowtan K (2004) Coot: Model-building tools for molecular graphics. *Acta Crystallogr D Biol Crystallogr* 60:2126–2132.
45. Chen VB, et al. (2010) MolProbity: All-atom structure validation for macromolecular crystallography. *Acta Crystallogr D Biol Crystallogr* 66:12–21.
46. Schrödinger (2017) *2017-2: MacroModel* (Schrödinger, New York).
47. Frisch MJ, et al. (2016) *Gaussian 09, revision A. 02* (Gaussian, Wallingford, CT).
48. Becke AD (1993) Density-functional thermochemistry. III. the role of exact exchange. *J Chem Phys* 98:5648–5652.
49. Lee C, Yang W, Parr RG (1988) Development of the Colle-Salvetti correlation-energy formula into a functional of the electron density. *Phys Rev B Condens Matter* 37:785–789.
50. Miertus S, Tomasi J (1982) Approximate evaluations of the electrostatic free-energy and internal energy changes in solution processes. *Chem Phys* 65:239–245.
51. Miertus S, Scrocco E, Tomasi J (1981) Electrostatic interaction of a solute with a continuum. A direct utilization of AB initio molecular potentials for the prevision of solvent effects. *Chem Phys* 55:117–129.
52. Pascualahuir JL, Silla E, Tunon I (1994) GEPOL: An improved description of molecular surfaces. III. A new algorithm for the computation of a solvent-excluding surface. *J Comput Chem* 15:1127–1138.
53. Grimme S, Ehrlich S, Goerigk L (2011) Effect of the damping function in dispersion corrected density functional theory. *J Comput Chem* 32:1456–1465.
54. Grimme S, Antony J, Ehrlich S, Krieg H (2010) A consistent and accurate ab initio parametrization of density functional dispersion correction (DFT-D) for the 94 elements H-Pu. *J Chem Phys* 132:154104.